Relationship Between Liver Size and Body Size[1]

FRANK H. DeLAND, M.D., and WENDY A. NORTH, M.I.R.

WITH THE ADVENT of newer technics for organ visualization such as radionuclide scanning, it is helpful to know the normal range of organ size relative to body size. Unfortunately, little information on this subject is available. For example, most references give the range of liver weight in the adult male or female without giving the relationship to body height or weight (1–5). In a series of autopsies, Stowens related liver weight to body height for children (6). The only data, however, on the relationship of liver weight and size to body weight, height, and/or surface in adults are the studies made by Frericks (7) of 24 persons. We selected, therefore, a series of 550 cases from 5,000 autopsy protocols of the Department of Pathology of The Johns Hopkins Hospital, plus 75 nonhospitalized autopsied cases (60 males and 15 females) from the files of the Medical Examiner's Office of the State of Maryland. From these cases studied, we were able to relate liver size to body size.

MATERIALS AND METHODS

The 550 cases were selected on the basis of the following criteria: (*a*) no clinical, laboratory, or autopsy evidence of hepatic pathology; (*b*) no evidence of cardiovascular disease, such as cardiac decompensation or increased peripheral venous pressure; (*c*) no evidence of systemic disease of the liver, such as infection, lymphoma, leukemia, or collagen disease.

These same criteria were used in the selection of the cases of the Medical Examiner. Such cases were limited to those persons dying instantaneously from gunshot wounds, severe crushing injuries, falls from high structures, or automobile accidents. Cases were not included if there was evidence of significant hemorrhage prior to death.

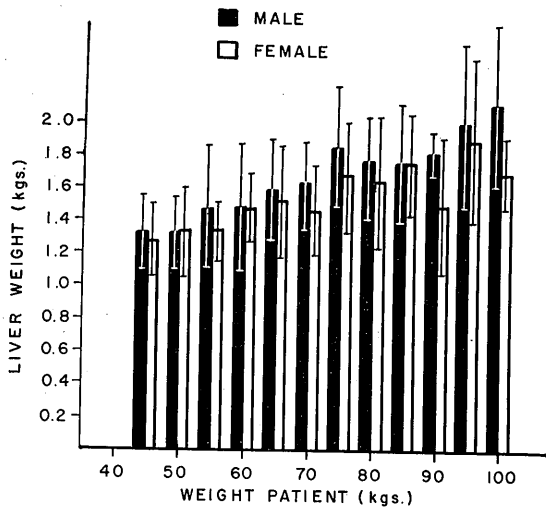

Fig. 1. The mean liver weight as a function of body weight. Each bar is the mean liver weight ± one standard deviation.

Data on age, sex, body weight and height, and liver weight were tabulated. Measurements of the width, height, and depth of the liver were made at the time of autopsy in only the hospital series. Body surface area was determined from a nomogram based on the formula of DuBois and DuBois (11):

$$\textit{Surface Area } (m^2) = \textit{weight } \frac{1}{2.35} \textit{ (kg)} \times \textit{height } \frac{1}{1.38} \textit{ (cm)} \times 6$$

RESULTS

Relationship Between Liver Weight and Body Weight: The body weights of the subjects were grouped in 5 kg increments. The mean liver weight (±1 S.D.) for each increment is shown in Figure 1. It can be seen that as body weight increases, the liver weight increases, but at a slower rate. According to Stahl (8), the relationship between body weight and organ weight in animals is more linear if one relates the exponential function of each. Therefore, the

[1] From the Division of Nuclear Medicine, The Johns Hopkins Medical Institutions, Baltimore, Maryland. Accepted for publication in June 1968.
This study was supported by U.S.P.H.S. Grant GM 10548.
RADIOLOGY 91:1195–1198, December 1968. (V.O.B.)

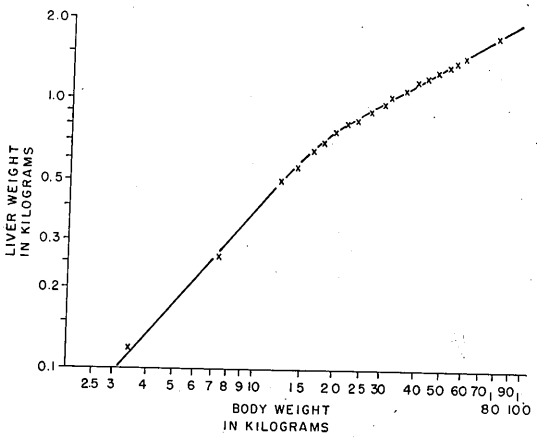

Fig. 2. The exponential of the mean liver weight as a function of the exponential of the body weight. Males and females are grouped together.

logarithm of body weight was plotted as the abscissa, and the logarithm of the mean liver weight as the ordinate (Fig. 2). For a body weight between 3 and 20 kg the relationship was a nearly straight line with a slope of about 45°. From 20–30 kg of body weight the rate of increase in liver weight decreased but remained nearly linear. The liver is reported to be 3.8 per cent of body weight at birth (9). We found this percentage to be maintained over the first 20 kg of growth (10). Thereafter, the decrease remained approximately linear, with the equation being:

$$\textit{Liver Weight (kg)} = \textit{Body Weight}/70 + 4/7.$$

The relatively smaller liver weight with respect to body weight above ten years of age may be related to the increase in the percentage of body fat, which is greater in the adult than in the child.

TABLE I summarizes the differences between sexes. From 45 to 100 kg of body weight, the liver was 6–7 per cent heavier in the male than in the female. This difference may also be due to differences in lean body mass between the sexes. The variation in liver weight for any specific body weight was approximately ±20 per cent (1 S.D.).

Relationship Between Liver Weight and Body Height: The cases were grouped in 5 cm increments of body height. The mean liver weight (±1 S.D.) for each increment is shown in Figure 3. TABLE I illustrates

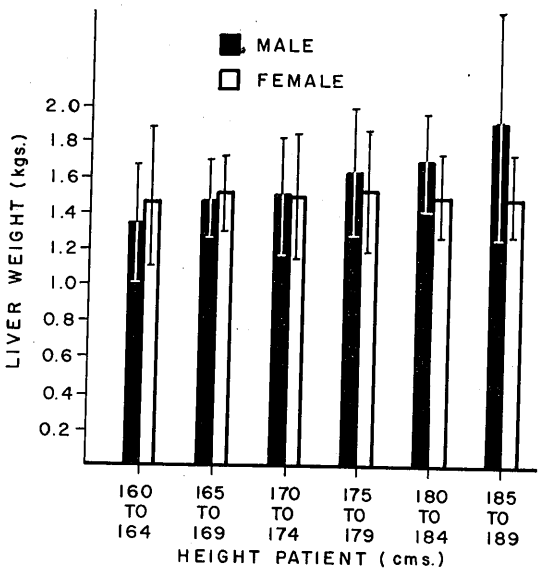

Fig. 3. The mean liver weight as a function of body weight. Each bar is the mean liver weight ± one standard deviation.

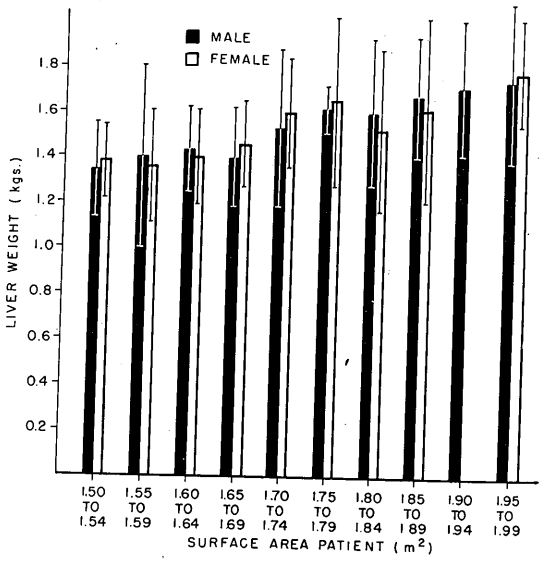

Fig. 4. The mean liver weight as a function of body surface area. Each bar is the mean liver weight ± one standard deviation.

that with increasing height, the liver was heavier in the male than in the female. For example, with an increase in height of 25 cm (from 160 to 185 cm) the liver of the male increased 36 per cent whereas the liver of the female increased only 22 per cent. The variation in liver weight for any specific height was approximately ±20 per cent (1 S.D.).

Relationship Between Liver Weight and Body Surface Area: Since body surface area is a function of both height and weight, either of which may vary separately, we correlated the liver weight with body surface as determined from the formula of DuBois and DuBois. The cases were grouped in increments of 0.05 square meters

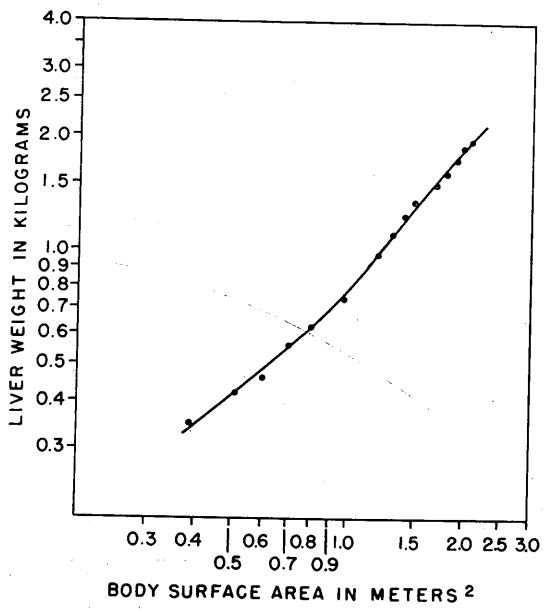

Fig. 5. The exponential of the mean liver weight as a function of the exponential of the body surface area. Males and females are grouped together.

of surface area. Figure 4 shows the mean liver weight (±1 S.D.) for each increment. One standard deviation of liver weight for any specific body area was ±16 per cent, slightly less than the variance of height or weight. Males and females had essentially the same liver weight for the same body surface area (TABLE I). The ratio of liver weight to body surface was fairly constant from infancy to approximately ten years of age (surface area of about 0.9 m^2). Above this range the liver was heavier in relation to surface area (Fig. 5).

Relationship of Liver Weight and Liver Dimensions: Height, width, and depth were measured in 507 of the hospital cases. These measurements represented the maximum dimensions of the organ for each case. If the liver is considered rhomboidal or pyramidal in shape, one can calculate the

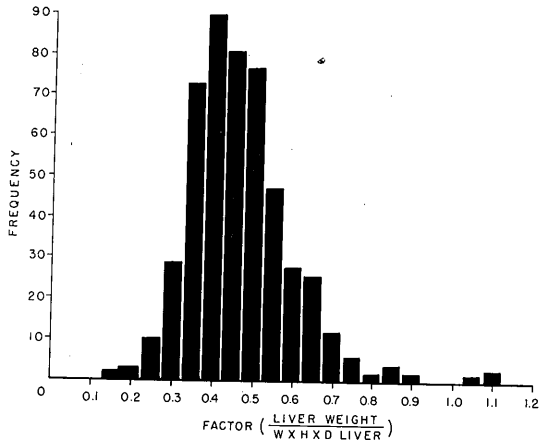

Fig. 6. Frequency bar graph of the ratio of liver weight to the product of liver dimensions. (Height × width × length).

TABLE I: A COMPARISON OF THE LIVER WEIGHT IN THE MALE AND FEMALE WITH RESPECT TO HEIGHT, WEIGHT, AND BODY SURFACE AREA

	Mean Liver Weight (kg)	
	Male	Female
Height		
160–164 cm	1.375	1.375
185–189 cm	1.875	1.675
Weight		
45–49 kg	1.250	1.250
95–99 kg	2.000	1.875
Surface area		
1.40–1.44 m^2	1.275	1.275
1.85–1.89 m^2	1.675	1.650

liver weight from these measurements with the formula:

$$Weight = K'(H \times W \times D)$$

Figure 6 shows the frequency distribution of K' over the entire range of liver weight. This factor averaged 0.48 with a standard deviation of ±0.19. This correlation is inadequate to be of much clinical value. If the configuration of the liver is considered to be a cone, the correlation between weight and dimensions is even less. There also was no correlation between frontal surface area of the liver, frontal plus lateral surface area, and liver weight.

Nomogram Relating Body Surface and Liver Weight: We were able to establish the normal range of liver weight with respect to body size. Since the relationship of body surface area to liver weight was essentially the same for males and for females, this was selected as the most re-

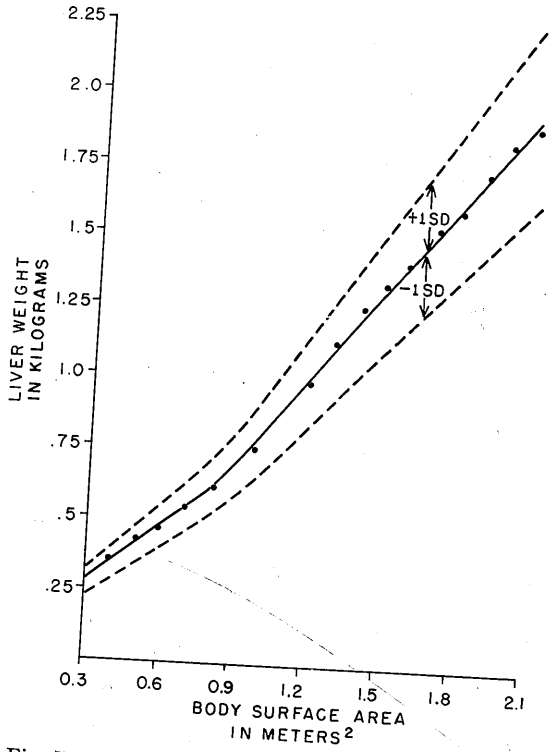

Fig. 7. Nomogram of liver weight as a function of body surface area. The solid line is the mean liver weight for both sexes and the dotted lines ± one standard deviation.

liable index. A graph correlating body surface with liver weight is shown in Figure 7. For those persons with a body surface area 1.0 m^2 or greater, the following equation can be used to calculate the liver weight in kilograms:

$$Y = 1.02\,X - 0.22$$

where:

Y = liver weight in kg

X = body surface area in m^2.

SUMMARY

In a series of 625 autopsies of adults without evidence of liver disease, the relationship between liver weight and body surface area (1.0 m^2 and greater) can be described by the equation:

Liver Weight (*kg*) =

1.02 body surface area (m^2) − *0.22*

Over the entire range of body surface area studied, the relative standard deviation of liver weight was 16 per cent. It was found that when body weight or height was correlated with liver weight a significant difference between males and females was observed. Males had larger livers than females for the same body weight or of the same height. These results showed that no clear-cut relationships between simple dimensions and weight of the liver could be ascertained in those persons with normal livers.

Johns Hopkins Medical Institutions
615 N. Wolfe St.
Baltimore, Md. 21205

REFERENCES

1. POPPER, H., AND SCHAFFNER, F.: Liver: Structure and Function. New York, Blakiston, 1957.
2. BRASH, J. C., ed.: Cunningham's Textbook of Anatomy. London, Oxford Univ. Press, 9th ed., 1951.
3. BOCKUS, H. L.: Gastroenterology. Philadelphia, W. B. Saunders, Vol. 3, 2d ed., 1965.
4. GARDNER, E., GRAY, D. J., AND O'RAHILLY, R.: Anatomy. Philadelphia, W. B. Saunders, 1960.
5. DAVIES, D. V., AND DAVIES, F., eds.: Gray's Anatomy. London, Longmans, Green, and Co. Ltd., 33d ed., 1962.
6. STOWENS, D.: Pediatric Pathology. Baltimore, The Williams and Wilkins Co., 2d ed., 1966.
7. FRERICKS, T.: A Clinical Treatise on Diseases of the Liver. London, New Sydenham Society, Vol. 1, 1860.
8. STAHL, W. R.: Organ Weights in Primates and Other Mammals. Science **150:** 1039–1042, Nov. 19, 1965.
9. NELSON, W. E.: Textbook of Pediatrics. Philadelphia, W. B. Saunders Co., 4th ed., 1945.
10. Unpublished data.
11. DUBOIS, D., AND DUBOIS, E. F.: A Height-Weight Formula to Estimate the Surface of Man. Proc. Soc. Exper. Biol. **13:** 77–78, 1916.

David P. DiPaolo, MD[2] • Robert A. Zimmerman, MD • Lucy B. Rorke, MD
Elaine H. Zackai, MD • Larissa T. Bilaniuk, MD • Anthony T. Yachnis, MD[3]

Neurofibromatosis Type 1: Pathologic Substrate of High-Signal-Intensity Foci in the Brain[1]

PURPOSE: **To investigate a correlation between pathologic and radiologic findings with regard to the characteristic high-signal-intensity foci seen on long repetition time (TR) magnetic resonance (MR) images of the brain in patients with neurofibromatosis type 1 (NF-1).**

MATERIALS AND METHODS: **Three girls with NF-1 and abnormal hyperintensities on long TR images of the brain underwent pathologic examination at autopsy.**

RESULTS: **Two 10-year-old girls had classic, focal hyperintensities in the internal capsules and globus pallidus regions, which have been associated with NF-1. The third patient, a neonate, had diffuse hyperintensity of the supratentorial and infratentorial white matter on T2-weighted MR images. Findings at histopathologic examination revealed spongiotic change in the tissue sections that correspond to the high-signal-intensity foci demonstrated on T2-weighted images.**

CONCLUSION: **Hyperintense foci seen on T2-weighted MR images appear to correspond to pathologic findings of areas of vacuolar or spongiotic change. The resultant fluid-filled vacuoles explain the occurrence of high signal intensity demonstrated on T2-weighted images.**

Index terms: Brain neoplasms, MR, 142.1214 • Basal ganglia, diseases, 142.1831 • Brain, white matter, 10.1831 • Neurofibromatosis, 142.1831

Radiology 1995; 195:721–724

NEUROFIBROMATOSIS type 1 (NF-1), or von Recklinghausen disease, is a syndrome with prominent cutaneous and central nervous system manifestations. NF-1 is a relatively common disorder, with a prevalence of roughly one in 3,000 individuals (1). Recent research in molecular genetics has revealed that NF-1 results from a mutation that involves the long arm of chromosome 17 (2). The responsible gene locus has a mutation rate that is among the highest for humans and is estimated to be approximately one in 10,000 gametes per generation (2). It is transmitted in an autosomal dominant fashion, but approximately 50% of cases represent new mutations. The pathogenesis of the disease appears to relate to inactivation of a tumor suppressor gene (3,4).

A wide variety of intracranial lesions are exhibited in patients with NF-1. Glial tumors of the optic nerve or pathway occur frequently (1,5), but the most common intracranial lesions in patients with NF-1 are high-signal-intensity foci seen on long repetition time (TR) magnetic resonance (MR) images. These foci with abnormal increased signal intensity on T2-weighted images, which occur in about two-thirds of patients with NF-1, are most commonly demonstrated in the basal ganglia, especially in the globus pallidus, cerebellum, internal capsule, and brain stem (1,5–7). These lesions are not associated with mass effect and do not enhance after administration of gadopentetate dimeglumine (8); however, the lesions in the globus pallidus occasionally have a mild mass effect and may be bright on T1-weighted images (5,8,9). It has been surmised that these abnormal high-signal-intensity foci are not neoplastic, but, to our knowledge, a conclusive correlation between radiologic and pathologic findings has not been established. These abnormal high-signal-intensity foci have been described as hamartomas (1,5,8), abnormal myelination (8), or heterotopias (1,10). The lack of a pathologic correlation has contributed to the confusion with regard to these lesions, particularly because spontaneous regression of some of these foci has been noted (5,11).

The purpose of our study was to investigate a correlation between pathologic and radiologic findings in three patients with clinically diagnosed NF-1. These patients, who had hyperintense lesions on long TR MR images, died of complications of their diseases. Necropsy was performed in all three patients, and the radiologic findings of high-signal-intensity foci were correlated with the pathologic findings.

CASE REPORTS

Patient 1.—A 10-year-old girl had a diagnosis of neurofibromatosis, restrictive lung disease, and severe cervicothoracic kyphoscoliosis. (The diagnosis of neurofibromatosis was made on the basis of café au lait spots and plexiform neurofibroma.) At 2 years of age, she underwent posterior spinal fusion with Harrington rod placement; at 2½ years of age, she underwent corrective surgery for a thoracic deformity.

At age 10 years, she was admitted to the hospital because of back pain and to undergo repair of a cosmetic deformity. She underwent further surgical intervention,

[1] From the Departments of Radiology (D.P.D., R.A.Z., L.T.B.), Neuropathology (L.B.R., A.T.Y.), and Genetics (E.H.Z.), the Children's Hospital of Philadelphia, 34th St and Civic Center Blvd, Philadelphia, PA 19104. From the 1994 RSNA scientific assembly. Received October 25, 1994; revision requested November 17; revision received January 27, 1995; accepted February 6. **Address reprint requests to** R.A.Z.

[2] Current address: Department of Radiology, Thomas Jefferson University Hospital, Philadelphia, Pa.

[3] Current address: Department of Pathology, Health Science Center, University of Florida College of Medicine, Gainesville.

Abbreviations: NF-1 = neurofibromatosis type 1, TE = echo time, TR = repetition time.

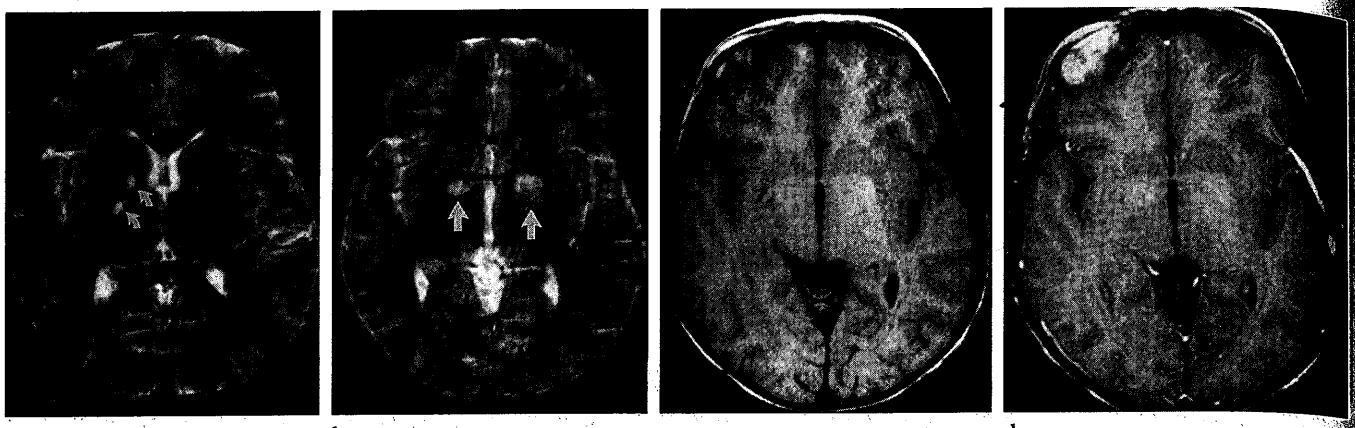

a. b. c. d.

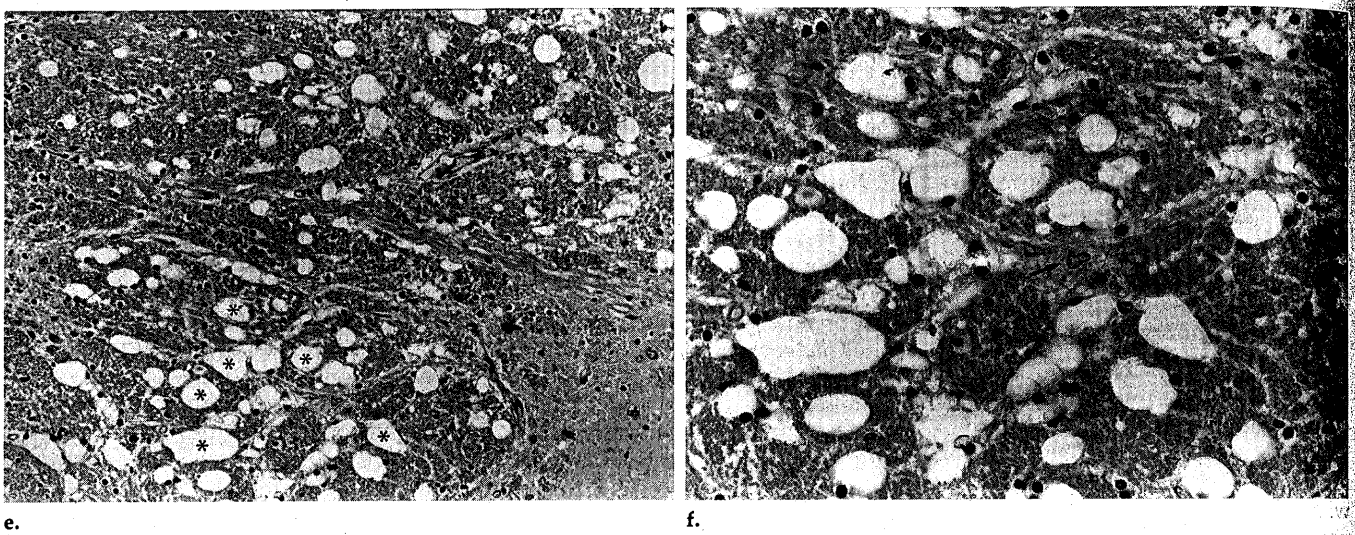

e. f.

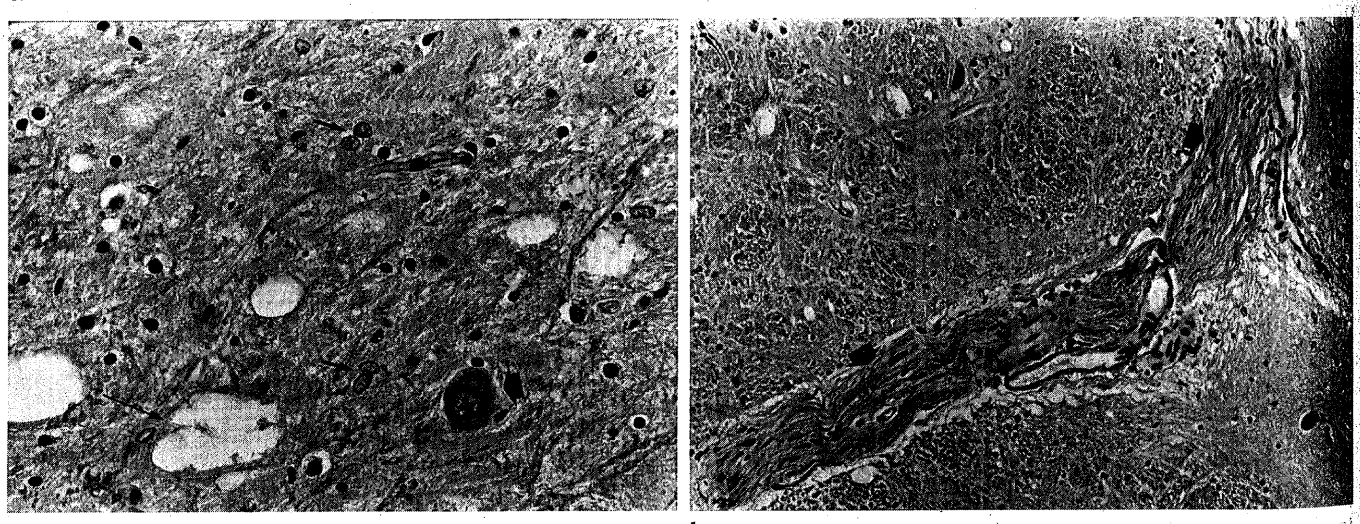

g. h.

Figure 1. Patient 1. **(a, b)** Axial 2,500/80 (long TR msec/echo time [TE] msec) MR images demonstrate focal hyperintensities in the right internal capsule (genu and posterior limb), as well as the medial globus pallidus nuclei bilaterally (arrows). **(c)** Axial short TR/TE (600/20) image shows increased signal intensity in the basal ganglia. **(d)** Postcontrast axial image shows no enhancement. **(e)** Photomicrograph of globus pallidus demonstrates multiple vacuoles (some of which are labeled with *) of variable size within the neuropil (hematoxylin-eosin stain; original magnification, ×100). **(f)** Photomicrograph with medium magnification of the same area in the pallidum shows multiple apparently empty vacuoles, in most cases with one or two adjacent oligodendroglia. Note the enlarged astrocyte nucleus with the abnormal configuration characterized by a crinkled "V" shape (arrow). There is no evidence of demyelination or inflammation (hematoxylin-eosin stain; original magnification, ×400). **(g)** Photomicrograph of the medial segment of the globus pallidus shows several vacuoles and two pairs of protoplasmic astrocytes (short, thin arrows). Coalescence of vacuoles is demonstrated (long, thin arrow). A normal neuron is also shown (thick arrow) (hematoxylin-eosin stain; original magnification, ×400). **(h)** Photomicrograph at low magnification of longitudinally sectioned Schwann cells (arrows) surrounding an intrinsic pallidal vessel. Several small vacuoles are distributed throughout the field of view (hematoxylin-eosin stain; original magnification, ×100).

but she died of hypoventilation and hypotension postoperatively.

MR images of the brain obtained when she was 8 years old demonstrated rounded, hyperintense foci on the long TR images in the basal ganglia and internal capsule, which are typically seen in patients with NF-1 (Fig 1a, 1b). These lesions were also mildly hyperintense on T1-weighted im-

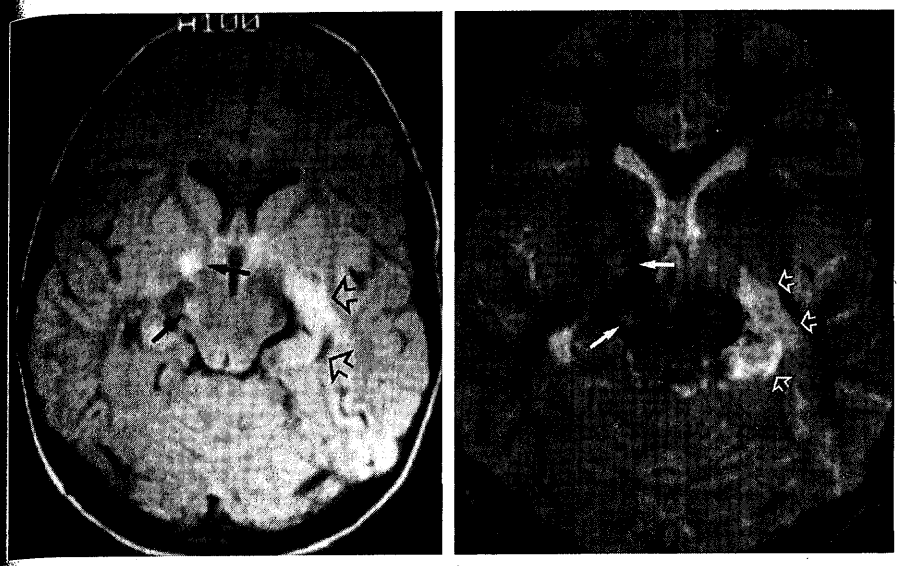

a. b.

Figure 2. Patient 2. **(a)** Axial long TR/short TE (2,500/30) and **(b)** long TR/TE (2,500/80) MR images demonstrate focal hyperintensities in the right globus pallidus, internal capsule, and crus cerebri (solid arrows). Increased signal intensity in the medial left temporal lobe (open arrows) is related to the patient's anaplastic astrocytoma, which was diagnosed at autopsy.

ages but were not associated with mass effect or contrast material enhancement (Fig 1c, 1d).

Findings from the pathologic examination of this patient's central nervous system revealed megalencephaly (brain weight of 1,530 g, compared with a normal weight of 1,290 g) without gross focal lesions. In addition to the routine histologic sections obtained at multiple levels of the neuraxis, serial sections of the globus pallidus were also examined. Results from microscopic examination (Fig 1e–1h) demonstrated diffuse proliferation of protoplasmic astroglia at all levels but particularly in the globus pallidus, substantia nigra, and dentate nucleus. In the globus pallidus, these glia frequently contained unusual, twisted or crinkled nuclei, which appeared to be reactive rather than neoplastic (Fig 1f). In addition, the globus pallidus and substantia nigra displayed an abnormal pallor on routine staining. Intrinsic pallidal vessels were cuffed by a ring of piloid astrocytes in the neuropil, and perivascular schwannosis immediately surrounding the small venules was noted (Fig 1h). Microcalcifications were present in areas of the pallidi. In addition to the glial proliferation, there was a spongy or vacuolar change in the internal capsule, which was adjacent to the pallidum; the cerebral peduncles; the deep cerebellar white matter, which was adjacent to the dentate nuclei; and the optic tracts. The vacuoles, which appeared to be within the myelin, measured 5–100 μm in diameter and did not contain any apparent stainable material. There were larger spaces that appeared to have resulted from the coalescence of smaller vacuoles. These extended focally into adjacent gray matter structures and incited no inflammatory or other tissue reaction as might be seen in a demyelinating disease. There was no evidence of axonal damage or obvious abnormalities of the oligodendrocytes. The tissue was stained for myelin and showed no evidence of demyelination in the affected areas. Suitable material was not available for ultrastructural studies; therefore, our suspicion of intramyelinic edema could not be confirmed.

Patient 2.—A 10-year-old girl with NF-1 had been well until the last year of her life, at which time she developed right-sided headaches, intermittent emesis, and seizures. Radiographic examinations performed at that time demonstrated findings of a right cerebellopontine angle mass; findings from lumbar puncture revealed pleocytosis and an elevated protein level. A pathologic diagnosis could not be made from the results obtained at cytologic examination of the cerebrospinal fluid. A posterior fossa craniectomy for limited tumor resection was performed, and a diagnosis of fibrosarcoma was made. The patient developed hydrocephalus postoperatively and underwent further surgery for placement of a ventriculoperitoneal shunt. The patient was given chemotherapy that consisted of vincristine sulfate (Oncovin; Lilly Laboratories, Indianapolis, Ind), doxorubicin hydrochloride (Adriamycin; Adria Laboratories, Columbus, Ohio), and cyclophosphamide (Cytoxan; Bristol-Meyers Squibb, Evansville, Ind). A few weeks later, the patient developed back and leg pain, as well as urinary retention. Computed tomographic (CT) myelography demonstrated subarachnoid spread of the tumor to the spine.

The patient was given palliative therapy and died several weeks later. Permission for restricted autopsy, which was limited to the brain and spine, was obtained from the parents.

There was a maternal family history of NF-1; a male sibling also had NF-1. The patient had multiple café au lait spots, as well as a plexiform neurofibroma of the neck. As described earlier, CT demonstrated enhancement of a mass in the right cerebellopontine angle with subarachnoid spread of tumor. Abnormal enhancement was also demonstrated in the medial left temporal lobe. T2-weighted MR images also depicted characteristic high-signal-intensity foci in the right globus pallidus, internal capsule, and the right midbrain (Fig 2). Tumor involvement was seen in the right seventh cranial nerve, the trigeminal ganglion, the fifth cranial nerve, the brain stem, and the upper cervical cord, as well as the left temporal lobe. At autopsy, histologic examination of the brain revealed findings of a diffusely infiltrative anaplastic astrocytoma with subarachnoid involvement.

Sections of the right globus pallidus and internal capsule showed a spongiotic change similar to that seen in patient 1, but it was less extensive. No stainable material was identified in these vacuoles. No gliosis or associated inflammatory tissue reaction was found. Findings from Bodian and Klüver-Barera staining methods revealed no evidence of demyelination.

Patient 3.—A female neonate was transferred to our institution shortly after birth. She was born at 34 weeks estimated gestational age to an 18-year-old primigravida, who had NF-1. The neonate developed a grade IV intraventricular hemorrhage, hydrocephalus, and seizures on the 1st day of life. A large mass on the left side of the face was noted at birth. Exophthalmos and buphthalmos of the left eye were also demonstrated at MR imaging.

The neonate's head circumference was 35 cm (50th percentile), and she weighted 2.5 kg (< 5th percentile). Physical examination revealed a soft, rubbery fullness over the left maxillary area. There was exophthalmos of the left eye and clouding of the cornea. No other palpable masses were present, and there were no cutaneous stigmata that are typically associated with neurofibromatosis. MR images demonstrated an extensive, enhancing mass that involved the soft tissues of the left side of the face, the left orbit, and cavernous sinus, as well as the soft tissues of the left side of the neck. A biopsy of the mass facilitated a diagnosis of plexiform neurofibroma, for which the infant was treated with vincristine and dactinomycin on the 48th day of life. The infant developed pneumonia and severe respiratory stridor, and intubation was necessary. She was extubated at the family's request and died at home at 14 weeks of age.

Findings on MR images obtained at our institution when the infant was 6 weeks old confirmed the presence of a large plexiform neurofibroma, which was similar to that demonstrated on images obtained at another institution. An interval increase in ventricular size was evident, along with evidence of previous hemorrhage. Buphthalmos and exophthalmos of the left eye were again noted. No focal signal intensity abnormalities in the basal ganglia, cerebellum, or brain stem were

seen on the long TR MR images; however, there was diffuse high signal intensity in the supratentorial and infratentorial white matter on the long TR images. Findings from the histologic evaluation of the cerebral cortex and white matter demonstrated a primary developmental abnormality, consisting of whorls of Schwann cells adjacent to some meningeal arteries, and areas of heterotopia. The white matter was characterized by areas of hypocellularity associated with status spongiosis throughout, in which astrocytes with small processes were scattered. This spongiotic change was the same as that noted in the previous two cases. Vacuoles were discovered throughout the white matter and measured 5–100 μm. No inflammatory reaction, gliosis, or axonal abnormalities were present.

DISCUSSION

The findings in this study of three patients with NF-1 indicate a consistent change in cerebral tissue that corresponds to abnormal high-signal-intensity foci seen on long TR MR images of the brain. Specifically, these lesions are characterized by spongiform myelinopathy or vacuolar change of myelin, in which vacuoles are identified that ranged from 5 to 100 μm in diameter. No stainable material is evident, which suggests that in life they are filled with water. The larger vacuoles and lesions appreciated on long TR MR images appear to represent a confluence or coalescence of smaller vacuoles. They did not incite inflammatory reaction in the tissue. There is no frank demyelination. If the vacuoles are filled with water, this would explain why the lesions are bright on T2-weighted images. Specifically, intramyelinic edema has a long T2 relaxation time; this would produce hyperintensity on T2-weighted images. Because intramyelinic edema appears to constitute the predominant pathologic change, hypointensity of the lesions on T1-weighted images might be expected; however, these foci tend not to be hypointense on T1-weighted images. It may be that the distance between vacuoles is large enough that partial volume effects intervene, and the long T1 of the fluid is averaged with adjacent tissue that has a shorter T1 relaxation time. These foci with abnormal increased signal intensity on T2-weighted images in NF-1 are also occasionally hyperintense on T1-weighted images, as described in patient 1 in our series. The microcalcifications seen in the globus pallidus regions at histologic examination in patient 1 may account for the increased signal intensity on T1-weighted images, since small calcifications have been described as a cause of T1 shortening (12). Henkelman et al (12) have demonstrated that calcium deposits in concentrations of up to 30% by weight in brain parenchyma can produce shortening of the T1 relaxation time owing to a surface relaxation mechanism.

It is unclear why the foci with abnormal increased signal intensity on T2-weighted images in the basal ganglia, brain stem, and cerebellum sometimes regress, but it suggests that the intramyelinic edema is an intermittent or transient phenomenon.

The protoplasmic astroglia with the crinkled nuclei demonstrated at histologic examination in patient 1 are thought to represent a nonspecific, reactive change. In the experience of two neuropathologists (L.B.R., A.T.Y.), such protoplastic astroglia with crinkled nuclei have been identified in the pallidi of otherwise normal brain specimens used as controls. In contrast, the perivascular schwannosis, also noted in patient 1, is a described malformation that occurs in patients with NF-1 (13).

In conclusion, this series provides a correlation between radiologic and pathologic findings with regard to high-signal-intensity foci on long TR MR images in patients with NF-1. Correlation of histopathologic findings among the three patients revealed a consistent intramyelinic spongiotic or vacuolar change. The resultant fluid-filled vacuoles explain the occurrence of high signal intensity on T2-weighted images. ■

References

1. Braffman BH, Bilaniuk LT, Zimmerman RA. The central nervous system manifestations of the phakomatosis on MR. Radiol Clin North Am 1988; 26:773–800.
2. Riccardi VM. The prenatal diagnosis of NF-1 and NF-2. J Dermatol 1992; 19:885–891.
3. Seizinger BR. NF 1: a prevalent cause of tumorigenesis in human cancers? Nat Genet 1993; 3:97–99.
4. Andersen LB, Fountain JW, Gutmann DH, et al. Mutations in the neurofibromatosis 1 gene in sporadic malignant melanoma cell lines. Nat Genet 1993; 3:118–121.
5. Aoki S, Barkovich AJ, Nishimura K, et al. Neurofibromatosis types 1 and 2: cranial MR findings. Radiology 1989; 172:527–534.
6. Hashimoto T, Tayama M, Miyazaki M, et al. Cranial MR imaging in patients with von Recklinghausen's disease (neurofibromatosis type I). Neuropediatrics 1990; 21:193–198.
7. DiMario FJ Jr, Ramsby G, Greenstein R, Langshur S, Dunham B. Neurofibromatosis type I: magnetic resonance imaging findings. J Child Neurol 1993; 8:32–39.
8. Smirniotopoulos JG, Murphy FM. The phakomatoses. AJNR 1992; 13:725–746.
9. Mirowitz SA, Sartor K, Gado M. High-intensity basal ganglia lesions on T1-weighted MR images in neurofibromatosis. AJNR 1989; 10:1159-1163.
10. Bognanno JR, Edwards MK, Lee TA, Dunn DW, Roos KL, Klatte EC. Cranial MR imaging in neurofibromatosis. AJR 1988; 151: 381–388.
11. Sevick RJ, Barkovich AJ, Edwards MSB, Koch T, Berg B, Lempert T. Evolution of white matter lesions in neurofibromatosis type 1: MR findings. AJR 1992; 159:171–175.
12. Henkelman RM, Watts JF, Kucharczyk W. High signal intensity in MR images of calcified brain tissue. Radiology 1991; 179:199–206.
13. Norman MG, Ludwin SK. Congenital malformations of the nervous system. In: Davis RL, Robertson DM, eds. Textbook of neuropathology. 2nd ed. Baltimore, Md: Williams & Wilkins, 1991; 207–280.